

Electrostatic charging of spray dried mannitol upon mixing and its impact on mixing homogeneity

Elektrostatische Aufladung von sprühgetrocknetem Mannitol beim Mischen und ihr
Einfluss auf die Mischgüte

Master Thesis

Masterarbeit zur Erlangung des akademischen Grades eines Diplomingenieurs in der
Studienrichtung Verfahrenstechnik an der Technischen Universität Graz.

Einreichdatum: 18.04.2013

Name: **Markus Maier**
Adresse: Griesplatz 24/12
8020 Graz
Mat. No.: 0631468

Institute for Process- and Particle Engineering, Graz
Technical University

Advisors: Dipl.-Ing. Stefan Karner

Mag. Dipl.- Ing. Dr. Eva- Maria Littringer

Univ.-Prof. Dr.rer.nat. habil.Ph.D Nora Anne Urbanetz

Eidesstattliche Erklärung

Deutsche Fassung:

Beschluss der Curricula-Kommission für Bachelor-, Master- und Diplomstudien vom 10.11.2008

Genehmigung des Senates am 1.12.2008

EIDESSTATTLICHE ERKLÄRUNG

Ich erkläre an Eides statt, dass ich die vorliegende Arbeit selbstständig verfasst, andere als die angegebenen Quellen/Hilfsmittel nicht benutzt, und die den benutzten Quellen wörtlich und inhaltlich entnommene Stellen als solche kenntlich gemacht habe.

Graz, am

.....

(Unterschrift)

Englische Fassung:

STATUTORY DECLARATION

I declare that I have authored this thesis independently, that I have not used other than the declared sources / resources, and that I have explicitly marked all material which has been quoted either literally or by content from the used sources.

.....

date

.....

(signature)

Danksagung

Hiermit möchte ich mich bei allen bedanken, die mir bei meiner Arbeit sehr behilflich waren.

Ich bedanke mich bei Prof. Nora Urbanetz, ohne ihr wäre die Arbeit nicht möglich gewesen. Ein besonderer Dank gebührt auch meinem Betreuer DI Stefan Karner, der mich tatkräftig unterstützt hat und immer für mich Zeit hatte, wenn es Probleme gab, und weiters bei Dr. Eva Littringer ohne ihr wären einige Themenbereiche erst gar nicht behandelt worden. Dank gilt auch allen meinen Kolleginnen und Kollegen am Institut, die mich herzlich in ihr soziales Feld integriert haben.

Außerdem möchte ich mich bei meiner Familie herzlich bedanken, die mir dies alles ermöglicht hat und natürlich auch bei meinen Freunden, die immer ein offenes Ohr für mich hatten.

Table of Contents

Table of Contents	iii
List of Figures	v
List of Tables	vi
List of Equations	vii
Abbreviations	viii
Nomenclatures	ix
Kurzfassung	xi
Abstract	xii
1 Introduction	1
1.1 Factors impacting electrostatic charge acquisition	3
1.2 Interparticle Forces	4
1.2.1 Forces based on Solid or Liquid Bridges	4
1.2.1.1 Solid Bridges	5
1.2.1.2 Liquid Bridges	5
1.2.2 Immaterial Bridges	6
1.2.2.1 Van-der-Waals forces	7
1.2.2.2 Electrostatic force	7
1.2.2.3 Adhesive forces and Weight as a function of distance	8
1.3 Triboelectric Model	12
1.4 Specific Surface: Indicator for Roughness	13
1.4.1 Inner Surface	13
1.4.2 Outer Surface	14
1.4.3 Gas Adsorption method	14
1.4.3.1 Measuring Principle	14

1.4.3.2	Adsorption Isotherm	14
2	Materials and Methods	18
2.1	Materials.....	18
2.2	Methods.....	19
2.2.1	Preparation of spray dried mannitol	19
2.2.2	Powder Characterization.....	20
2.2.2.1	Strength Test.....	20
2.2.2.2	Roughness	21
2.2.2.3	Particle Size Distribution (PSD).....	21
2.2.2.4	Powder Density	21
2.2.2.5	Bulk and Tapped Density	22
2.2.2.6	Specific Surface Area.....	22
2.2.2.7	Flowability.....	23
2.2.3	Measurement of electrostatic charge	24
2.2.3.1	Measurement of electrostatic charge without API in stainless steel vessels	25
2.2.4	Electrostatic charge measurement with API in stainless steel vessels .	26
2.2.5	Mixing Quality	27
2.2.6	Construction of the Climate Box.....	27
2.2.6.1	List of Materials	27
2.2.6.2	Construction	28
2.2.6.3	Mechanism and function of the saturated salt solution.....	29
2.2.6.4	Generation of the constant relative humidity in the climate box by saturated salt solutions	30
2.2.7	Statistical Analysis	31

3	Results and Discussion	33
3.1	Particle Characterization	33
3.1.1	Strength Test	33
3.1.2	Particle Size Distribution	34
3.1.3	Roughness.....	36
3.1.4	Specific Surface Area	37
3.1.5	Bulk and tapped density.....	37
3.1.6	Powder Density.....	39
3.1.7	Flowability	39
3.2	Measurement of Electrostatic Charge of Mannitol without API in a stainless steel vessel	42
3.3	Measurement of Electrostatic Charge with API in a stainless steel vessel ..	43
3.4	Measurement of the Mixing Uniformity	45
4	Summary	47
5	Conclusion and Outlook	48
6	Bibliography.....	A
7	Appendix	D

List of Figures

Figure 1: Solid Bridges (Stieß 2008).....	5
Figure 2: Liquid Bridges (Stieß 2008)	5
Figure3: Immaterial Bridges.....	7
Figure 4: Pattern for adhesion calculation (Stieß 2008).....	8
Figure 5: Comparison between Adhesion/Weight depends on Particle Size and Contact Gap (Stieß 2008).....	10
Figure 6: Triboelectric Model (Lüttgens 2005)	12

Figure7: Inner surface (Stieß 2008).....	13
Figure8: Outer surface (Stieß 2008).....	13
Figure9: Adsorption isotherm "Type 2" (Stieß 2008)	15
Figure 10: BET-Line and its simplification (Stieß 2008).....	16
Figure 11: Adsorption apparatus (schematically) (Stieß 2008).....	17
Figure 12: Experimental Set up, Flowability.....	23
Figure 13: Electrostatic charge measurement set up	24
Figure 14: Climate box (SolidWorks Academic Version)	28
Figure 15: Exchange of water molecules (Clark 2004)	29
Figure 16: Smooth powder after sieving	34
Figure 17: Smooth powder after mixing.....	34
Figure 18: Rough powder after sieving.....	34
Figure 19: Rough powder after mixing.....	34
Figure 20: Particle size distribution of the rough and smooth powder determined by laser diffraction, n=3, MV	35
Figure 21: Scanning electron micrograph of the smooth powder.....	36
Figure 22: Scanning electron micrograph of the rough powder	36
Figure 23: a) Released mass smooth powder; b) Released mass rough powder.....	40
Figure 24: Electrostatic charge carried by mannitol in stainless steel vessel without API, n=3 (MV \pm SD)	42
Figure 25: Electrostatic Charge carried by mannitol in Stainless steel vessel with API, n=3 (MV \pm SD)	43
Figure 26: Mean standard deviation of the API content (MV \pm SD ,n=3)	46

List of Tables

Table 1: Spray drying conditions	20
Table 2: Set the relative humidity in a temperature range of 15-30 ° C (Lide 2006-2007)	31
Table 3: Parameters of the PSD, n=3, MV \pm SD.....	36
Table 4: Bulk and Tapped density, n=3, MV \pm SD	38
Table 5: Released mass smooth powder	41
Table 6: Released mass rough powder	41

Table 7: API content of the samples taken from 3 independent adhesive mixtures (mean \pm SD of n=10)	45
---	----

List of Equations

Equation1: Van-der-Waals; Plate/Sphere	9
Equation2: Van-der-Waals; Sphere/Sphere.....	9
Equation 3: Electrostatic Force- Conductor; Plate/Sphere	9
Equation 4:Electrostatic Force- Conductor; Sphere/Sphere	9
Equation 5: Electrostatic Force- Insulator; Plate/Sphere	9
Equation 6: Electrostatic Force- Insulator; Sphere/Sphere	9
Equation 7: Weight force of a sphere	10
Equation 8: BET-isotherm.....	15
Equation9: BET Line.....	16
Equation10: Linear equation.....	16
Equation 11: Simplification	16
Equation 12: Monolayer capacity.....	17
Equation13: Hausner Ratio.....	38

Abbreviations

API	Active Pharmaceutical Ingredient
BET	Brunnauer Emmett Teller
DPI	Dry Powder Inhaler
HPLC	High Pressure Liquid Chromatography
MDI	Metered Dose Inhaler
PP	Poly Propylene
PSD	Particle Size Distribution
PVC	Poly Vinyl Chloride
RH	Relative Humidity
rpm	Revolutions per Minute
SD	Standard Deviation
SEM	Scanning Electron Microscope
SS	Salbutamol Sulphate
MV	Mean Value

Nomenclatures

μm	Micrometer
\AA	Ångström
$h\omega$	Van-der-Waals Interaction Energy
π	PI (3,14...)
d	sphere diameter
a	(smallest) distance between plate/sphere, sphere/sphere
F_{dw}	Van der Waal Force
F_{cond}	Electrostatic force (conductor)
F_{insul}	Electrostatic force (insulator)
ϵ_0, ϵ	permittivity of vacuum, relative dielectric constant
U	contact potential at electric conductors
φ_1, φ_2	surface charge density of the plate/sphere, sphere/sphere
F_g	Gravity Force
ρ_s	Density Solid
g	Gravitational Acceleration
F_H	Adhesive Force
nm	Nano Meter
n	adsorbed amount of gas
nm	monolayer capacity
C	dimensionless constant

pr	Pressure Ratio
p, p ₀	Pressure
%RH	Relative Humidity in Percent
P	Probability
m	Meter
w%	weight Percentage
°C	Degree Celsius
l/h	Liter per Hour
g	Gram
min	Minute
h	hour
ml	MiliLiter
pH	Activity of the Hydrogen Ion
mm	Mili Meter
m ² /g	Square Meter per Gram
g/ml	Gram per MiliLiter
mg	Mili Gram
g/cm ³	Gram per Cubic Centimeter
nC/g	Nano Coloumb per Gram
mg/g	Mili Gram per Gram

Kurzfassung

In dieser Masterarbeit wurde die elektrostatische Aufladung von Mannitolpartikeln mit unterschiedlicher Oberflächenrauheit in einem Mischprozess untersucht. Die Versuche wurden sowohl mit den Mannitolpartikeln allein als auch mit ihren interaktiven Mischungen mit mikronisiertem Salbutamolsulfat durchgeführt. Schließlich wurde der Einfluss der elektrostatischen Aufladung auf die Mischungsgüte der interaktiven Mischung beurteilt.

Vor den Untersuchungen zur Elektrostatik und der Mischungsgüte wurden die verschieden rauen Pulver auf ihre Rauheit, Festigkeit, Partikelgröße, Dichte, Schütt- und Stampfdichte, spezifische Oberfläche sowie auf ihre Fließfähigkeit untersucht. Bei der Fließfähigkeit zeigte sich ein signifikanter Unterschied zwischen dem rauen und dem glatten Pulver.

Um die elektrostatischen Versuche unter definierten Raumbedingungen durchführen zu können, wurde eine Klimabox konstruiert und gebaut. Mit einer Kalium Carbonat Lösung wurde ein konstantes Klima in der Box sichergestellt.

Die Mischversuche wurden mit einem Edelstahl Mischbehälter durchgeführt. Nach dem Mischvorgang wurde das durchmischte Pulver in der Klimabox in einem Faraday Becher auf seine elektrostatische Ladung mit Hilfe eines Hoch-Widerstands-Elektrometers bestimmt. Die Versuche im Edelstahl Behälter zeigten einen signifikanten Unterschied zwischen dem rauen und dem glatten Pulver. Das raue Pulver lud sich mehr auf als das glatte. Bei den Versuchen mit den interaktiven Pulvern zeigte sich kein Unterschied in der elektrostatischen Aufladung, doch aber ein Unterschied in der Mischungsgüte. Das glatte Mannitol Pulver hatte eine bessere Mischungsgüte als das raue weil das Aufladeverhalten des Trägers die Mischungsgüte beeinflusst.

Abstract

In this thesis, the electrostatic charging behavior of mannitol with two different surface roughnesses was determined in stainless steel mixing vessels. Furthermore, experiments with adhesive mixtures with special focus on the electrostatic charging habit and on the quality of mixing were performed. The adhesive mixtures consisted of mannitol and micronized salbutamol sulphate. Prior to the charge measurements these two different rough powders were characterized regarding their roughness, strength, particle size, density, bulk and tapped density, specific surface area, and their flowability. Whereby, the flowability showed a significant difference between the rough and the smooth powders. To be able to perform electrostatic experiments a climate box was designed and built. With a potassium carbonate solution a constant climate in the box was generated. Electrostatic experiments were carried out with stainless steel mixing vessels. After blending the powder in a turbular blender the electrostatic charge was determined in a Faraday cup with a high-resistance electrometer. The tests in stainless steel vessels showed a significant difference between the rough and the smooth powder. The rough powder showed a higher charge magnitude than the smooth powder. In experiments with adhesive powders there was no difference in electrostatic charge magnitude but a difference in mixing uniformity between these two mannitol types. The smooth powder showed a better mixing uniformity than the rough powder. A reason for a different mixing homogeneity could be that mixing uniformity is influenced by the charging behaviour of the carrier

1 Introduction

In today's time drug delivery to the lungs becomes more and more important as the pulmonary route offers advantages over other administration routes, such as the oral and the parenteral route. Many people, including especially pediatric and geriatric patients, have problems with swallowing conventional solid dosage forms. Parenteral delivery of injections frequently decreases patient compliance due to pain sensitivity. A solution of these problems is drug delivery by inhalation. There are several advantages with pulmonary drug delivery, including increased acceptance by the patients due to easy and convenient administration. Furthermore, the pulmonary route guarantees the bypassing of the gastrointestinal tract. Thus, API degradation prior to reaching its target in the human body is suppressed, which leads to an efficient medical therapy. Evermore pharmaceutical companies are formulating active pharmaceutical ingredients (APIs) for pulmonary therapies.

There are three common devices for drug delivery to the lungs. These are nebulizer, metered dose inhaler (MDI) and dry powder inhaler (DPI). In this work a DPI was used, therefore the nebulizer and the MDI are not of further interest. Since the API particles of DPIs have to show an aerodynamic diameter between 0.5 and 5 μm for pulmonary administration (Labiris&Dolovich et. al, 2003), the flowability and the dosing uniformity are negatively impacted. Thus, for DPIs there are principally two possibilities, without any focus on dosing and ensuring deposition of the API, to deposit the API in the pulmonary region of the human lung. The first possibility is to prepare an adhesive powder mixture, in which the small API particles stick on larger carrier particles. The second possibility is to form larger agglomerates of the small API particles. In this thesis the focus is laid on the first possibility. Common carriers

are lactose, glucose and mannitol (Saint-Lorant, Leterme, Gayot, & Flament, 2007; Steckel & Bolzen, 2004). The typical range for the size of the carrier is 50 μm – 200 μm (Labiris & Dolovich, 2003).

After being released from the DPI the adhesive powder mixture follows the air stream into the mouth where the small (API) and the large (carrier) particles have to separate. The larger carrier particles impact in the mouth or in the throat, while the small API particles follow the air stream through the bronchial into the alveolar region of the lung. The alveoli are small bubbles, which are located at the end of the bronchia. Drug deposition in the lungs is caused by several mechanisms, i.e., impaction, sedimentation, Brownian diffusion and electrostatic deposition (Gonda et al, 1992). The driving force for impaction is inertia. Sedimentation is caused by gravity, which leads to settling of particles in the lung. Brownian diffusion takes place in the vesicles of the alveoli. In the alveoli the small particles (smaller than 1 μm) get in contact with gas molecules. This interaction between particles and gas molecules can lead to deposition of small particles on the alveoli walls.

During formulation development of DPIs two major issues are of concern, i.e., the uniformity of the adhesive mixture and the uniformity of the released dose. These characteristics are impacted by inter-particle forces, especially the electrostatic and Van der Waal forces.

In this thesis the main focus was on the investigation of the impact of electrostatic forces on the mixing homogeneity. Electrostatic forces arise in solid systems by contact electrification (Rowley et al 2001). Electrostatic charging (triboelectrification) is a complex phenomenon. The contact pressure, area, time and frequency between two solids are mostly unknown and very hard to find out. The main problem during the mixing process is that charged particles may experience repulsive forces and

incline to stick on the wall of the blending vessel both deteriorating mixing homogeneity.

In the present work mannitol was used as carrier and salbutamol sulphate (SS) was used as API. The adhesive powder mixture was prepared in a Turbula® blender and the electrostatic charging was determined in dependence on the carrier roughness which is one of the most important powder properties in DPI technology.

1.1 Factors impacting electrostatic charge acquisition

The main part of this master thesis concerns the electrostatic charge acquisition of powders upon mixing. During mixing the electrostatic charging behavior of the powder plays an important role because interparticle interactions between the components of the mixture impacting for example mixing homogeneity are dependent on electrostatic charges that may be carried by the powders involved. Sign and magnitude of the electrostatic charge are difficult to predict or rather poorly understood. The charging process is influenced by many parameters, such as:

- surface conductivity affected by relative humidity
- particle size and shape (P.A. Carter et al 1998)
- impurities (Eilbeck et al 1999, Eilbeck et al 2000, Murtomaa et al 2001)
- temperature,
- contacting materials (Elajnaf et al 2006, Adi 2010)
- mixing speed (energy of contact), (Wantanabe et al 2006,2007)
- mixing time,

-
- specific surface and contact area which is affected by surface roughness and particle size (Karner et al 2012)

As discussed above, a higher surface roughness results in a higher specific surface area. That means if two powders with the same particle size distribution (PSD) but two different surface roughnesses were tumbled, the rougher powder has an ability to take up more charge until charge saturation than the smooth powder.

1.2 Interparticle Forces

For inhalation powders interparticle forces have a great impact on the performance of the inhalate. One of these performance criteria is mixing uniformity.

There are many approaches available in literature describing the phenomenon of interparticle forces such as capillary forces, van-der-Waals forces and electrostatic forces. The most important forces will be discussed in this chapter.

Interparticle forces may be divided in forces based on solid or liquid bridges and forces based on immaterial bridges.

1.2.1 Forces based on Solid or Liquid Bridges

Forces based on solid bridges are subdivided in sinter bridges or melting bridges and crystallized solids, those based on liquid bridges in adsorption layers and capillarity.

1.2.1.1 Solid Bridges

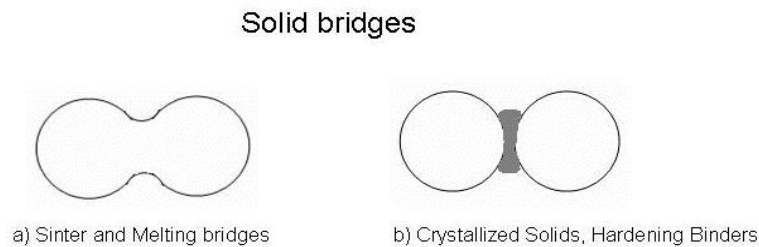


Figure 1: Solid Bridges (Stieß 2008)

Solid bridges may be developed because of sintering and melting processes at the surface of two or more particles on the one hand and crystallized solids and hardening binders at the surface on the other hand. In Figure 1 both kinds of solid bridges are shown. Sintering and melting processes can occur when the temperature on the contact line is approximately 60% of the absolute melting temperature and when there is enough contact time, e.g. during compressing (Stieß 2008).

1.2.1.2 Liquid Bridges

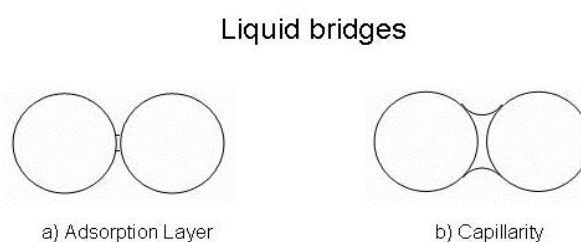


Figure 2: Liquid Bridges (Stieß 2008)

Liquid bridges can be divided in bridges caused by adsorption layers (Figure 2a) and capillarity (Figure 2b). Adsorption layers can be seen as a transition from solid to liquid bridges. The layer thickness of these bonds is less than 3 nm and adsorption layers are able to dissolve the solid. Upon drying the dissolved solid is able to form a solid bond. The dominant forces are the cohesion force of the binder and the adhesion force on the solid, see chapter 1.2.1.1.

Capillarity is formed by the presence of a liquid between the particles. The adhesive forces are mainly based on surface forces which are caused by surface tension at the contact line of the liquid bond and by the capillary pressure inside the liquid bond. When the curvature of the surface is concave as shown in Figure 2b, a low pressure dominates inside the liquid bond and therefore the particles attract each other (Stieß 2008).

The main focus of this thesis is on the investigation of the forces based on immaterial bridges, especially the electrostatic force which is described in the following chapter.

1.2.2 Immaterial Bridges

In general, the forces based on immaterial bridges are divided into Van-der-Waals forces, electrostatic forces and form-fit bonds. Since spherical particles are used in this study form-fit bonds are irrelevant for this thesis.

Adhesion Forces

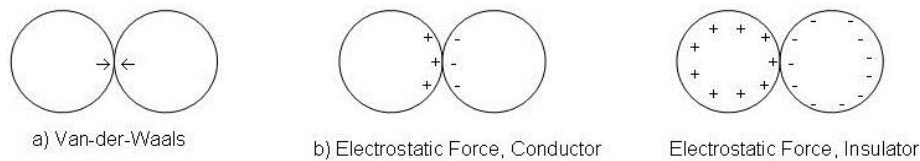


Figure3: Immaterial Bridges

1.2.2.1 Van-der-Waals forces

Van-der-Waals forces are based on dipole interactions between atoms and molecules of contacting surfaces (Figure3a). Although these forces are short ranging they are of great importance for small and dry particles which are in close contact. They may be altered by the presence of sorption layers on the surface of the particle as well as by surface roughness. Different surface roughness leads to different contact areas which increase or decrease the Van-der-Waals interaction (Stieß 2008). Furthermore, the distance between particles and therefore the Van-der-Waals interaction depends on the surface roughness.

1.2.2.2 Electrostatic force

Electrostatic attraction occurs between inversely charged surfaces, as shown in Figure3b and Figure3c. Electric conductors are charged due to electron transfer (contact potential), while insulating materials are charged due to friction, comminution and the like. Because of the diverse charge-discharge behaviour their adhesion

behaviour is different in each case (Stieß 2008). The adhesion behaviour is discussed in more detail in the following chapter.

1.2.2.3 Adhesive forces and Weight as a function of distance

In Figure 4 a pattern for the adhesion forces calculation is shown. The corresponding equations are displayed from Equation 1 to Equation 6. This approach is only valid for ideal pure and smooth surfaces and distances between 4 \AA and 500 \AA . The model cases in Figure 4 have little practical relevance because of their idealizations, but show the essential relationships. These are model cases for particle/wall adhesion and for particle/particle adhesion. Plate/plate contact has been neglected because of irrelevance in this case (Stieß 2008).

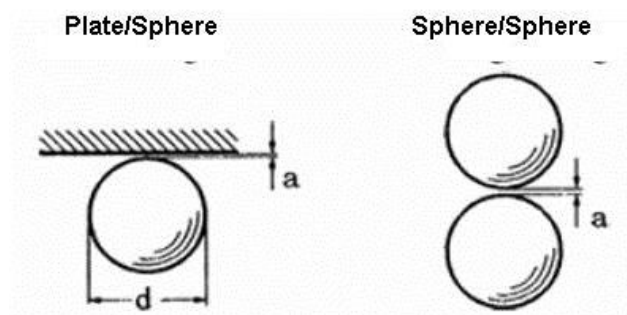


Figure 4: Pattern for adhesion calculation (Stieß 2008)

$$F_{vdW} = \frac{h\omega}{16 \cdot \pi} \cdot \frac{d}{a^2}$$

Equation 1: Van-der-Waals; Plate/Sphere

$$F_{vdW} = \frac{h\omega}{32 \cdot \pi} \cdot \frac{d}{a^2}$$

Equation 2: Van-der-Waals; Sphere/Sphere

$$F_{cond} = \frac{\pi}{2} \cdot \varepsilon_0 \cdot \varepsilon \cdot U^2 \cdot \frac{d}{a}$$

**Equation 3: Electrostatic Force- Conductor;
Plate/Sphere**

$$F_{cond} = \frac{\pi}{4} \cdot \varepsilon_0 \cdot \varepsilon \cdot U^2 \cdot \frac{d}{a}$$

**Equation 4: Electrostatic Force- Conductor;
Sphere/Sphere**

$$F_{insul} = \frac{\pi}{2} \cdot \frac{\varphi_1 \cdot \varphi_2}{\varepsilon_0 \cdot \varepsilon} \cdot d^2$$

**Equation 5: Electrostatic Force- Insulator;
Plate/Sphere**

$$F_{insul} = \frac{\pi}{4} \cdot \frac{\varphi_1 \cdot \varphi_2}{\varepsilon_0 \cdot \varepsilon} \cdot \frac{d^2}{\left(1 + \frac{a}{d}\right)}$$

**Equation 6: Electrostatic Force- Insulator;
Sphere/Sphere**

- hω van-der-Waals interaction energy (hω~5 eV~8·10⁻¹⁹ Nm)
- a (smallest) distance between plate/sphere, sphere/sphere
- d sphere diameter
- ε₀ permittivity of vacuum (ε₀=8.855·10⁻¹² AS/Vm; 1 AS/Vm=1N/V²)
- ε relative dielectric constant (ε=1 for vacuum)
- U contact potential at electric conductors (typical values 0.1...0.7 V)
- φ₁=φ₂ surface charge density of the plate/sphere, sphere/sphere

In Figure 5 the comparison between adhesion forces and weight force depending on particle size and contact gap for particle/wall adhesion is displayed. In Equation 7 the calculation of the weight force for a spherical, ideal particle is shown.

$$F_g = \frac{\pi}{6} \cdot \rho_s \cdot g \cdot d^3$$

Equation 7: Weight force of a sphere

- ρ_s density of the solid
- g gravity constant ($g=9.81 \text{ m/s}^2$)
- d sphere diameter

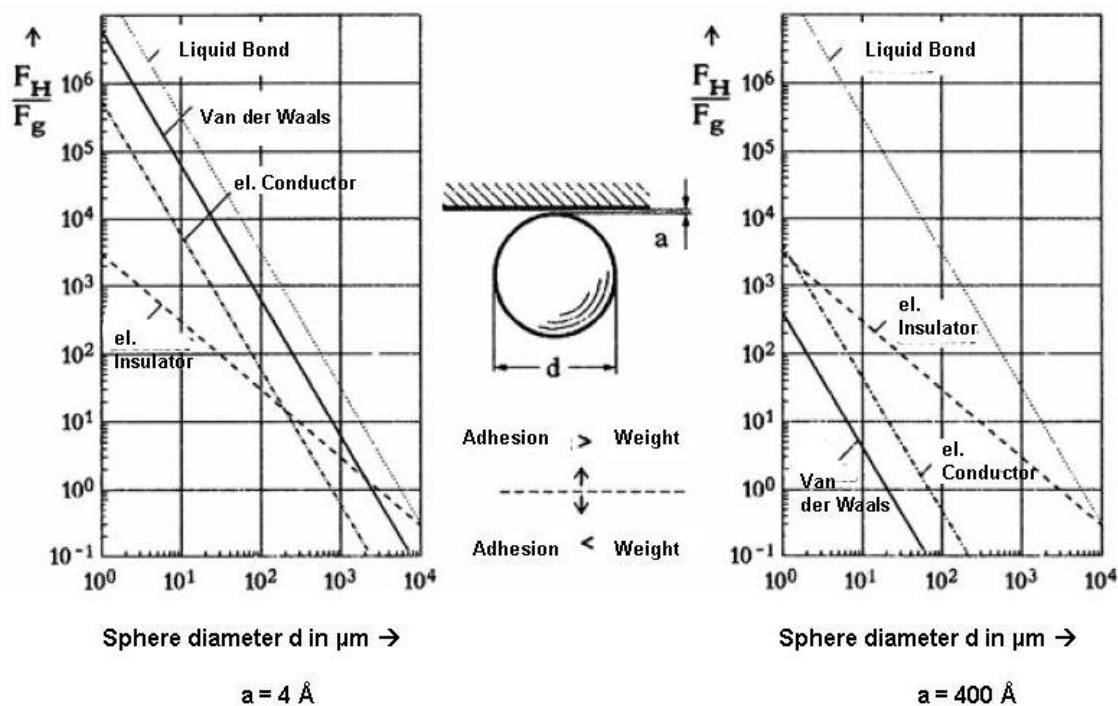


Figure 5: Comparison between Adhesion/Weight depends on Particle Size and Contact Gap (Stieß 2008)

The comparison from Figure 5 for the case particle/wall adhesion is performed by using following values: $\rho_s=3 \text{ g/cm}^3$, $U=0.5 \text{ V}$, $\varphi_1=\varphi_2=100 \text{ e}/\mu\text{m}^2=1.6 \cdot 10^{-5} \text{ N}/(\text{Vm})$. This

comparison shows that under ideal conditions practically every smooth sphere under a diameter of 1 mm should adhere on a smooth wall, the smaller the particle the stronger the bond to the wall. For particles with a diameter under 100 μm the weight force should become theoretically negligible. In practice the adhesion forces are distinctly smaller, this is because real bodies are not perfectly smooth but exhibit some kind of surface roughness that results in an increase of the distance a . For example, a sphere is brought to the distance of 500 \AA (surface roughness), the Van-der-Waals adhesion force is reduced by the factor of $6.4 \cdot 10^{-5}$ and the electrostatic adhesion force is reduced by the factor of $8 \cdot 10^{-3}$. Such distances and even greater distances are the reason for nearly disappearing of both forces. The liquid bonds were not treated (Stieß 2008).

1.3 Triboelectric Model

The term “triboelectric” derives from the Greek word τριβω (tribo), which means to rub something. It suggests that only friction may cause charging. However, this is not true, because electron transfer may take place whenever different materials get into contact. Nevertheless, friction favours/enhances the contact of surfaces. The theory behind electron transfer developed by Helmholtz (1879) is the so called double-layer charge. This theory is based on the fact that electrons may escape from a solid surface when an adequate energy input (e.g. heating) is provided. The energy required to emit electrons from the surface in a vacuum is the so called electron work function. Electrically insulating materials (acceptor) exhibit higher electron work functions than metals (donator). Metals always possess sufficiently free moveable electrons (Lüttgens 2005). In

Figure 6 the electron transfer is displayed schematically.

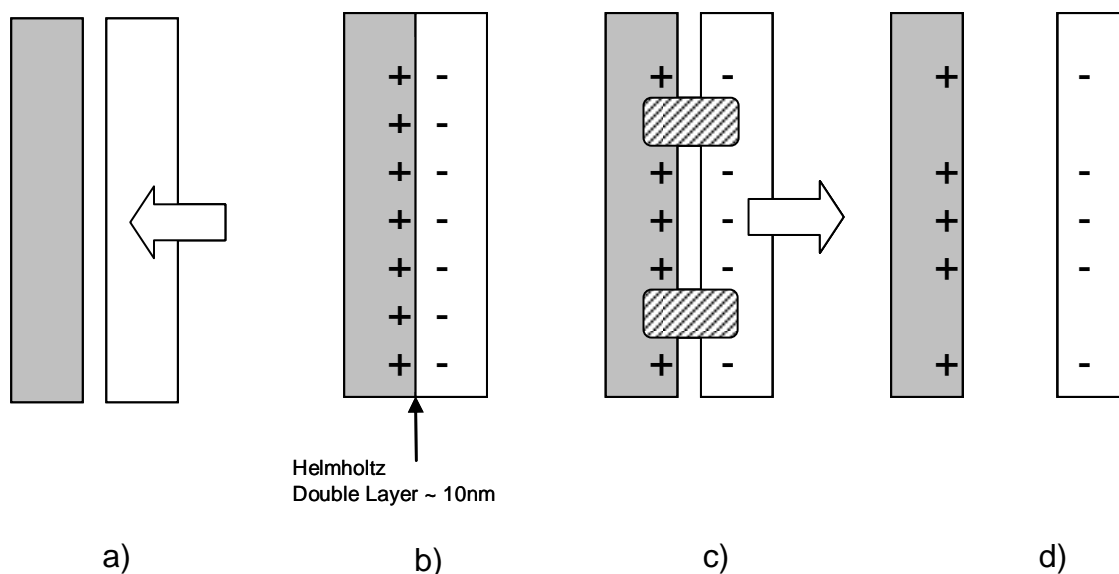


Figure 6: Triboelectric Model (Lüttgens 2005)

1.4 Specific Surface: Indicator for Roughness

The surface of finely dispersed substances has a great impact on chemical and physico-chemical processes, e.g. particle adhesion for instance during flow processes of fine grained bulk materials out of bins and silos (Stieß 2008).

Furthermore, the specific surface is an indicator for the roughness. The higher the specific surface, the rougher the particles are.

Depending on the used measurement principle the outer or the inner surface can be measured.

1.4.1 Inner Surface

The inner surface displays all pores, which are available to the measurement method (i.e., open pores) and includes the outer surface.

Therefore, methods that measure the inner surface usually provide much higher values than those that measure the outer surface. In Figure7 and Figure 8 the inner and outer surface are shown (Stieß 2008).



Figure7: Inner surface (Stieß 2008)



Figure8: Outer surface (Stieß 2008)

1.4.2 Outer Surface

The outer surface only contains the geometric structure of the particles, i.e. neither pores nor roughness.

In praxis three main measurement methods are used. These are the gas adsorption, flow-through process and the photometric method. In the present study the gas adsorption method was used.

1.4.3 Gas Adsorption method

1.4.3.1 Measuring Principle

The molecules of the inert measuring gas (e.g. N_2 , Ar, CO_2) bind, because of physisorption (without a chemical bond), on the surface of the porous and fine dispersed solid. Due to the inert behaviour of the measuring gas to the solid, the amount of adsorbed measuring gas only depends on the accessible surface of the sample (Stieß 2008)

1.4.3.2 Adsorption Isotherm

The adsorption isotherm describes the empirical relationship between the overall adsorbed amount of gas on the solid and the equilibrium pressure over the solid sample in the gas phase at a certain temperature.

There are different basic types of such adsorption isotherms. For the most common type ("Type 2", see Figure9), Brunauer, Emmet and Teller (BET) had described a physical and statistical relationship, the "BET- isotherm" (see Equation 8) .

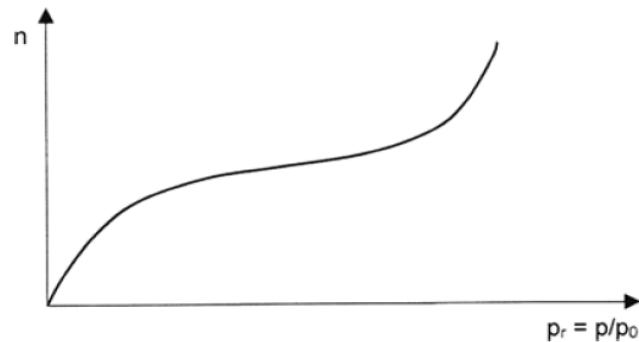


Figure9: Adsorption isotherm "Type 2" (Stieß 2008)

$$\frac{n}{n_m} = \frac{C \cdot p_r}{(1 - p_r) \cdot (1 - p_r + C \cdot p_r)}$$

Equation 8: BET-isotherm

n adsorbed amount of gas in Mol

n_m monolayer capacity in Mol

C dimensionless constant (includes the adsorption energy)

p_r ratio of p (measured gas pressure over the sample) and p_0 (saturation vapour pressure of the measuring gas at a certain measuring temperature)

Equation 8 shows a good accordance to the measured adsorption isotherm in a range of $0.05 < p_r < 0.3$.

Equation 8 transformed into a linear equation gives Equation9 (see Figure 10).

$$\frac{p_r}{n \cdot (1 - p_r)} = \frac{1}{n_m \cdot C} + \frac{C - 1}{n_m \cdot C} \cdot p_r$$

Equation9: BET Line

$$y = a + b \cdot x$$

Equation10: Linear equation

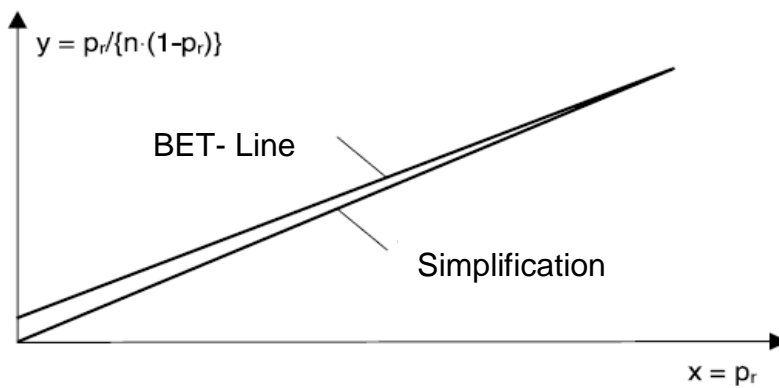


Figure 10: BET-Line and its simplification (Stieß 2008)

1.4.3.2.1 Simplification (Single Point Method)

For technical applications the constant C is usually much larger than 1 ($C \gg 1$). Therefore, the intercept a is negligible and thus Equation 9 can be simplified to Equation 11.

$$\frac{p_r}{n \cdot (1 - p_r)} = \frac{1}{n_m} \cdot p_r \rightarrow y = \frac{1}{n_m} \cdot x$$

Equation 11: Simplification

From this relation follows the monolayer capacity, which is the inverse value of the slope of the linear equation (see Equation 12)

$$n_m = n \cdot (1 - p_r) = \frac{x}{y}$$

Equation 12: Monolayer capacity

Thus, the line is placed through the origin, so only one point of the adsorption isotherm is enough to determine the slope of the line. This point, however, should be in the upper range of validity, so that the accuracy loss remains within the measurement error.

1.4.3.2 Adsorption Apparatus

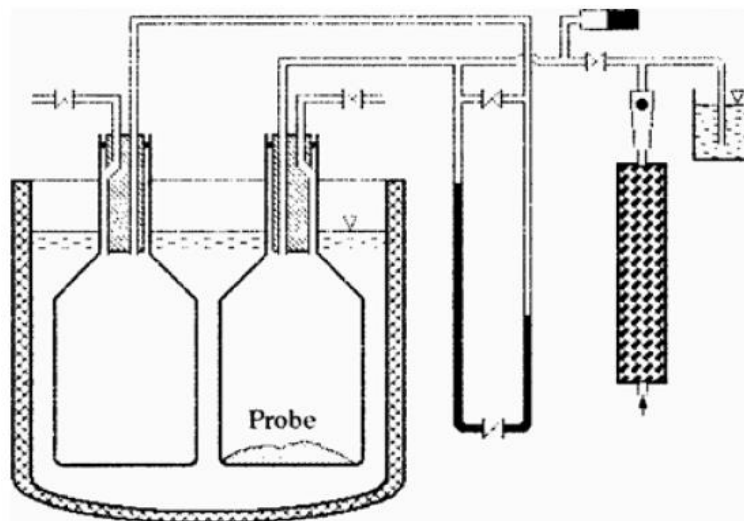


Figure 11: Adsorption apparatus (schematically) (Stieß 2008)

Figure 11 shows an adsorption apparatus. There are two vessels with the same volume. One of them contains the sample and the other one is empty. Both will be filled with nitrogen at room temperature and ambient pressure. In the next step these two vessels will be closed against each other and the environment. By cooling of the

two vessels in a liquid nitrogen bath, nitrogen adsorption takes place in the vessel which contains the sample. That's the reason why the pressure in the vessel with the sample decreases to a lower level than in the empty vessel. From the pressure difference, the weighing and the ambient pressure the mass-specific surface can be calculated.

2 Materials and Methods

2.1 Materials

Spray dried mannitol with two different surface roughnesses has been prepared according to Littringer et al 2012. The mannitol was spray dried in a pilot-scale co-current spray dryer. The 63 μm – 125 μm size fraction of both powders was obtained by mechanically sieving using a sieve shaker (Analysette®, Fritsch, Germany) according to DIN 6615. As API, micronized SS (USP25 quality) was used. SS was purchased from Selectchemie AG (Selectchemie AG, Switzerland) and micronized using an air jet mill (Alpine 50 AS, Hosokawa, Germany). The injection pressure was 6.0 bar and the milling pressure was 2.0 bar. A feed rate of 1 g/min was used. The particle size distribution of the API was analyzed using laser diffraction technique (HELOS/KR, Sympatec GmbH, Germany). The powder was dispersed in the dry state (injection pressure was 1 bar and feedrate was 30%) (Helos with Rodos dry dispersing unit, Sympatec GmbH, Germany). After milling the API showed the characteristic diameters $x_{10,3} = 0.46 \mu\text{m}$, $x_{50,3} = 1.69 \mu\text{m}$, $x_{90,3} = 5,65 \mu\text{m}$. Furthermore, micronized SS was used for the measurements of the electrostatic

charge of the adhesive mixtures and the mixing homogeneity. Potassium carbonate was used to generate the constant relative humidity of 43 %RH in the climate box (see chapter 2.2.6). Deionized water and ethanol was used to clean the mixing vessels prior the measurements of electrostatic charge and the mixing quality. Liquid nitrogen and helium was used for the measurement of the specific surface. Helium was further used for the density measurements. Acetic acid was used for adjusting the pH value for the eluent for the HPLC measurements for the mixing quality measurements. A Faraday cup, consisting of a cylindrical inner cup and a cylindrical outer cup (both made of stainless steel), divided by an insulating TeflonTM cup was used for charge measurement. As mixing vessels 75 ml stainless steel containers were used. The 75 ml stainless steel vessel had an inner diameter of 49 mm and an inner height of 40 mm. The faraday cup was connected to a high resistance electrometer (Keithley 6517B, Keithley Instruments Inc.,USA). For the statistical analysis and the graphics a statistic computer program was used (SigmaPlot 12[©], Systat Software, Inc., USA).

2.2 Methods

2.2.1 Preparation of spray dried mannitol

The preparation of spray dried mannitol was performed by Eva Littringer according to the procedure described in Littringer (2012). She used a pilot-scale co-current spray dryer with a diameter of 2.7 m and an overall height of 3.7 m. The concentration of

the solution for spray drying was amounted to 15 w% mannitol in water. The rough and the smooth powders were produced under different conditions. These conditions are shown in Table 1.

Table 1: Spray drying conditions

	Inlettemperature [°C]	Outlettemperature [°C]	Flow rate [l/h]
smooth	132	81	10
rough	131	71	20

2.2.2 Powder Characterization

2.2.2.1 Strength Test

The first investigation of the spray dried mannitol was to ensure that each powder could stand the sieving and mixing process without breaking. Therefore, each powder was pictured before and after sieving and mixing with a light microscope (Leica 4000, Leica Microsystems Inc., USA). Analyses before and after powder treatment were compared in order to determine the amount of broken particles.

2.2.2.2 Roughness

To evaluate the roughness of the two powder samples the particles were analyzed using a scanning electron microscope (Hitachi H-S4500 FEG, Hitachi High-Technologies Europe, Germany).

2.2.2.3 Particle Size Distribution (PSD)

The particle size distribution (PSD) of the 63 μm – 125 μm size fractions of the rough and smooth powder were investigated by laser diffraction in the dry state (Helos/KR and Rodos Sympatec GmbH, Clausthal- Zellerfeld, Germany). The powder dispenser was operating at 1 bar and 30 % feedrate. Each powder was measured in triplicate and was subdivided with a rotary cone divider to assure a representative sample prior to the measurement.

2.2.2.4 Powder Density

The powder density of each powder was determined by helium pycnometry (Accu-200 PycII 1340, Micromeritics, Germany). To condition the samples prior to the measurement they were dried in a dry oven at 40°C for 12 hours. The samples were measured in triplicate and to ensure a representative sample, the powders had been subdivided with a rotary cone divider before measurement.

2.2.2.5 Bulk and Tapped Density

The bulk and the tapped density were investigated according to the European pharmacopoeia (bulk and tapped density of powder Ph. Eur. 7.0) using method 1. The sample size was reduced to 3 g as the available amount of the powder was limited. A 10 ml graduated measuring glass instead of the compendial 100 ml graduated measuring glass was used. The volume before and after 1250 taps was recorded. The Hausner ratio was calculated to determine the powder flowability.

The powders were measured in triplicate and to ensure a representative sample, the powders were subdivided with a rotary cone divider before measurement.

2.2.2.6 Specific Surface Area

The specific surface area was determined using nitrogen adsorption (ASAP 2000, Micromeritics, US). The specific surface area was calculated according to Brunauer – Emmett – Teller (BET).

The samples were degassed at a temperature of 40°C before measuring. This temperature was chosen according to preliminary studies to ensure that the spray dried mannitol does not undergo any changes. The degassing time depended on the moisture content of the samples was set according to Littringer et al (2012) (at least 24 h).

Each powder was measured in triplicate and to ensure representative samples the powder were subdivided with a rotary cone divider before measurement.

2.2.2.7 Flowability

The flowability was measured by measuring the released dose per actuation and the uniformity of these released doses from a dry powder inhaler (Novolizer[®], MEDA Pharma GmbH & Co. KG, Germany) which was filled with 1 g of the mannitol powder. The measuring setup consisted of a vacuum pump (SV 1025C 000 IKXX, Busch, Switzerland), that sucked the dose out of the actuated inhaler, a connection tube, the sampling apparatus, in which the dose was collected, a mouthpiece for the inhaler and a filter paper (Type A/E, 47 mm, PALL GmbH, Dreireich, Germany) ensuring that the whole dose was captured in the sampling apparatus and was not transferred into the pump. An illustration of this setup is shown in Figure 12. The released mass was determined by weighing the inhaler before and after each actuation. This procedure was repeated 50 times for each powder. Each powder was measured in triplicate. The standard deviation is an indicator for the flowability. The air flow rate was set to 78.2 l/min to be consistent with the guidelines of the European Pharmacopoeia (powders for inhalation, Ph. Eur., 7.0). Suction time was set to 3 seconds to ensure that the total volume of air sucked through the inhaler is 4 l.

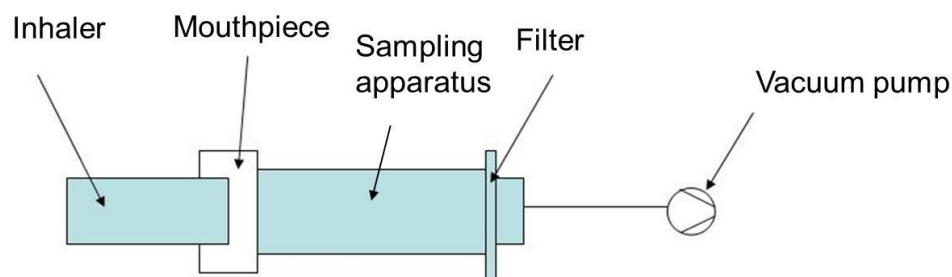


Figure 12: Experimental Set up, Flowability

2.2.3 Measurement of electrostatic charge

Charge measurement was performed using a Faraday cup (proprietary construction) connected to a high resistance electrometer (Keithley 6517 B, Keithley Instruments, USA). The cup consists of two cups of stainless steel which are placed into each other and separated from each other by a thick-walled jar made of Teflon™. The outer cup (protection cup) is grounded and works as a shield to protect the inner cup (measuring cup) from external influences. When a charged powder is poured into the inner cup, its charge induces a charge with the same magnitude but opposite polarity in the conducting material of the cup. Thus the charge of the powder can be calculated by measuring the voltage between the inner cup and the ground using an electrometer with known capacitor. Figure 13 shows an illustration of the used Faraday cup.

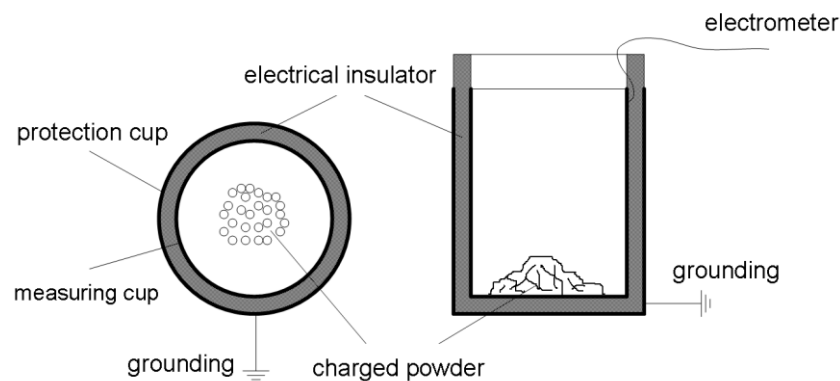


Figure 13: Electrostatic charge measurement set up

2.2.3.1 Measurement of electrostatic charge without API in stainless steel vessels

First the samples were stored for at least 3 days in stainless steel vessels in a climate box to ensure complete electrostatic discharge and to equilibrate the samples at constant and defined conditions of 43 %RH at room temperature. Sample size was set to 5 g. After conditioning the samples were sealed air tight.

Afterwards the closed vessels were taken out of the climate box and mounted on a tumble blender (T2F Turbula®, Willy A. Bachofen AG - Maschinenfabrik, Switzerland) and blended for 20 min at 60 rpm. In order to avoid charge exchange between the operator and the mixing vessel a protection cover, made of an electrical insulator, was used. After mixing, the vessels were taken back into the climate box where charge measurement was performed. The high resistance electrometer had to be switched on at least 2 hours before measurement to reduce variations of the measurement signal. Before and after charge measuring the inner Faraday cup was weighed to calculate the powder mass poured into the cup and the mass-specific netcharge carried by the powder. Per measuring cycle each powder was measured in triplicate.

2.2.4 Electrostatic charge measurement with API in stainless steel vessels

The micronized SS was first passed through a 250 μm sieve to remove large agglomerates. After this procedure the salbutamol sulphate was stored for at least 24 h in a desiccator. In the next step 2.5 g of spray dried mannitol was weighed into the stainless steel mixing vessel. Then, 0.125 g of micronized SS was added. After this, another 2.5 g of mannitol was weighed into the stainless steel vessel. The ratio of API and carrier was 1:40. In the next step, the three samples were stored 3 days in a climate box with a constant relative humidity of 43%RH. After these three days, each sample was blended in a Turbular[®] blender (T2F Turbula[®], Willy A. Bachofen AG - Maschinenfabrik, Switzerland). To ensure homogeneity, the powder was blended for 20 min at 60 rpm. In order to avoid charge exchange between the operator and the mixing vessel a protection cover, made of plastic, was used. After mixing, the vessels were taken back into the climate box where charge measurement was performed. The high resistance electrometer had to be switched on at least 2 hours before measurement to reduce variations of the measurement signal. Before and after charge measuring the inner Faraday cup was weighed to calculate the powder mass poured into the cup and the mass-specific netcharge carried by the powder. Per measuring cycle each powder was measured in triplicate.

2.2.5 Mixing Quality

To investigate the mixing uniformity 10 samples in a range of 10 mg to 20 mg were taken out of the Faraday Cup. Three samples were taken from the top, four from the middle and three from the bottom. Each of these 10 samples was dissolved in 10 ml deionized water with a pH of 3 (generated with acetic acid). After this, the samples were analyzed using a HPLC device (HP1090, Aglient technologies, Germany).

This procedure was made in triplicate for each powder.

2.2.6 Construction of the Climate Box

2.2.6.1 List of Materials

- Plexiglas®
- a pair of gloves (Glovebox)
- pipe coupling
- 2 socket plugs
- alumina angle rods
- silicone
- one blower with adapter
- bin for the salt solution
- 2 PVC pipe sections for the gloves

2.2.6.2 Construction

The climate box was built up of Plexiglas® tiling and alumina angle rods at the edges of the box in order to ensure good stability of the construction. It has the dimension 500 x 500 x 500 mm. In order to realize material input and output without destroying the climate inside the chamber, it has a sluice. The sluice consists of a cube with the dimension 250 x 250 x 250 mm and a pipe section with 2 cover plates. In Figure 14 the climate box is displayed.

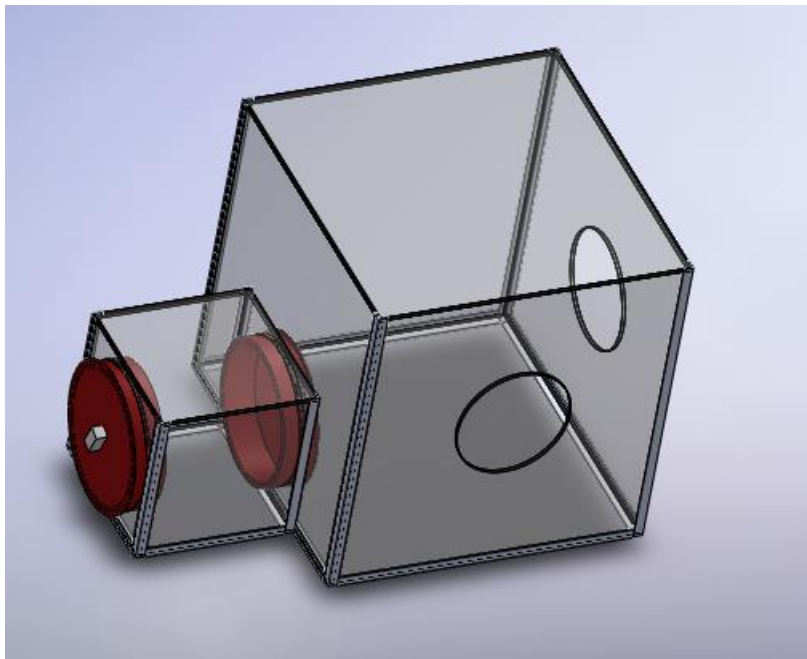


Figure 14: Climate box (SolidWorks Academic Version)

2.2.6.3 Mechanism and function of the saturated salt solution

The principle of regulating the RH with saturated salt solutions is simple. Any salt solution has its characteristic vapor pressure hence the relative humidity (RH) is less than over pure water. The reason for those phenomena is that the salt molecules only exist in the solution and not in the gas phase. Furthermore, there is an exchange of water molecules between the solution and the air in the box until the mechanism attains equilibrium. For that reason the RH is less than 100% (Lide 2006 - 2007). The interactions between the water molecules and the salt ions are strong. That's the reason why water molecules remain on the surface of the saturated salt solution. In Figure 15a) the molecule exchange of water molecules between the surface and the air and in Figure 15b) the exchange of water molecules in a saturated salt solution are pictured (Clark 2004).

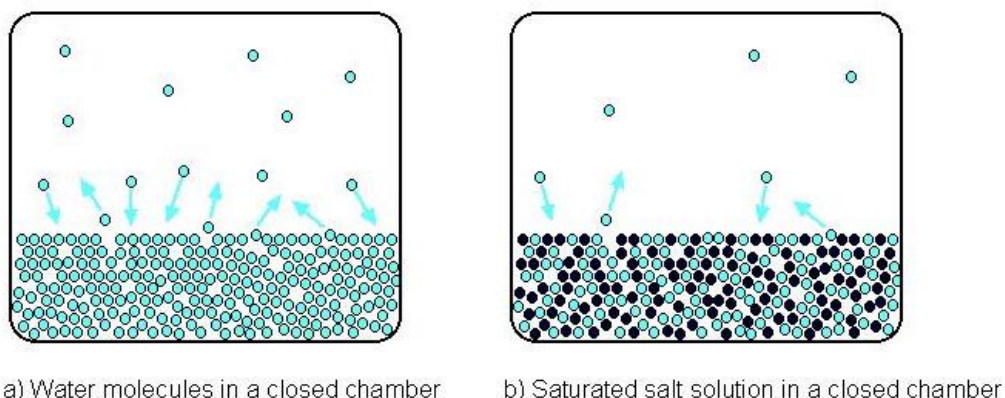


Figure 15: Exchange of water molecules (Clark 2004)

It is also advantageous that saturated salt solutions generate a constant RH as long as undissolved crystals of the salt are present. A major disadvantage is that salt solutions show a poor performance in dehumidifying. Saturated salt solutions pick up water from the air in the environment and that's the reason why this solutions start to dilute at their surface of the liquid. In consequence the diluted solution at the surface is lighter than the rest of the bulk and thus decomposition takes place. As a result, the RH on the surface of the solution increases to 100 %RH. Therefore it's important to require leakproofness of the box (Lide 2006 - 2007).

The accuracy of the relative humidity generated by saturated salt solutions is confirmed as they are used to calibrate hygrometers in the relative humidity (RH) fixed point method (Greenspan 1976). They were also used in museums to protect paintings and humidity sensitive items (OIML 1996).

2.2.6.4 Generation of the constant relative humidity in the climate box by saturated salt solutions

The preparation of the saturated salt solution is the main element of this experimental set-up. The salt should be free of impurities. The solution is made of distilled or deionized water and hygroscopic salt (in this work potassium carbonate K_2CO_3). Potassium Carbonate generates a relative humidity of approximately 43 %RH at room temperature. Table 2 shows the saturated RH-levels of several soluted salts

(Lide 2006-2007). K_2CO_3 was chosen because its saturation level at approximately 43 %RH match very well with standard room conditions.

During the preparation of the solution 30 % - 90 % of the salt should remain undissolved since the salt absorbs water from the air and thus the saturated solution would be diluted (OIML 1996). A non-saturated solution would not be able to generate constant relative humidity.

Table 2: Set the relative humidity in a temperature range of 15-30 ° C (Lide 2006-2007)

Temperature [°C]	MgCl ₂ [%]	K ₂ CO ₃ [%]	Mg(NO ₃) ₂ [%]	NaCl [%]
15	33,30 ± 0,33	43,2 ± 0,3	55,87 ± 0,27	75,61 ± 0,18
20	33,60 ± 0,28	43,2 ± 0,3	54,38 ± 0,23	75,47 ± 0,14
25	33,47 ± 0,24	43,2 ± 0,4	52,89 ± 0,22	75,29 ± 0,12
30	33,30 ± 0,21	43,2 ± 0,5	51,40 ± 0,24	75,09 ± 0,11

2.2.7 Statistical Analysis

For the statistical analysis a statistical computer program (SigmaPlot 12[®], Systat Software, Inc., USA) was used. A statistical t-test was performed to prove that there is a statistical significant difference. To prove the difference, the P- value was set to 0.05 and the confidence intervals were set to 95 %.The standard error, t and P values are approximations computed at the final iteration of the regression.

To compare the uniformity of the released powder mass of the smooth and the rough the standard deviation of the released mass of each cycle (50 actuations) was determined. A mean value of the three deviations of the three performed cycles for each experiment was calculated. The measure of the flowability is the mean of the scattering of the released powder masses of the 50 actuations.

To compare the mixing qualities of both powders the standard deviation of the API content in 10 samples taken from a mixture was determined. The experiments were performed in triplicate. The measure of the mixing quality is the mean of the standard deviation of the API content in the 10 samples mentioned above.

3 Results and Discussion

3.1 Particle Characterization

The particle characterization of the carrier particles is crucial for further experiments. The particle strength, the particle size distribution, the roughness, the specific surface area, the bulk and tapped density and the powder density (He- density) were determined.

3.1.1 Strength Test

Prior to the further measurements the particles were examined under a light microscope to prove that the particles had not broken during sieving that was a pretreatment of the particles before further investigations (according to chapter 2.2.2.1). This is crucial for further experiments. Additionally, particle integrity was investigated after mixing in the tumble blender.

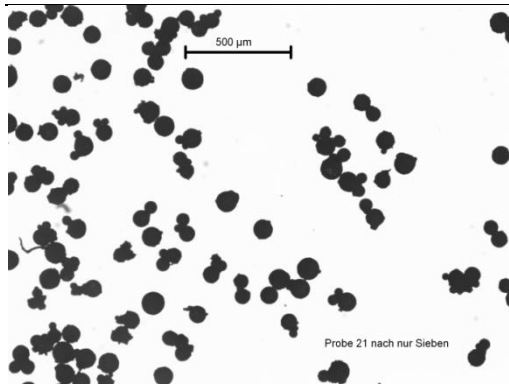


Figure 16: Smooth powder after sieving

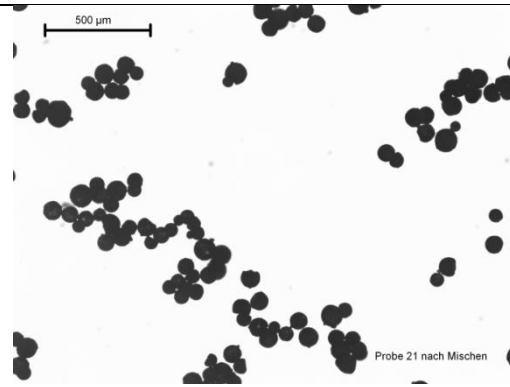


Figure 17: Smooth powder after mixing



Figure 18: Rough powder after sieving

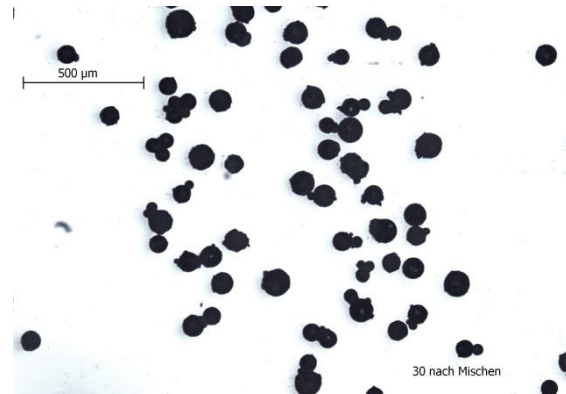


Figure 19: Rough powder after mixing

In Figure 16 to Figure 19 it is shown that the particles of the smooth powder and rough powder did not break during mixing and sieving.

3.1.2 Particle Size Distribution

The particle size of the size fractionated powders was checked (according to chapter 2.2.2.3) to ensure that the yield fraction was between 63 μm and 125 μm. The particle size distribution (PSD) was determined using laser diffraction (Helos, Sympatec GmbH, Clausthal- Zellerfeld, Germany) using the dry dispersion system

Rodos (Sympatec GmbH, Clausthal- Zellerfeld, Germany). In Figure 20 the PSD of the smooth powder and the rough powder are shown.

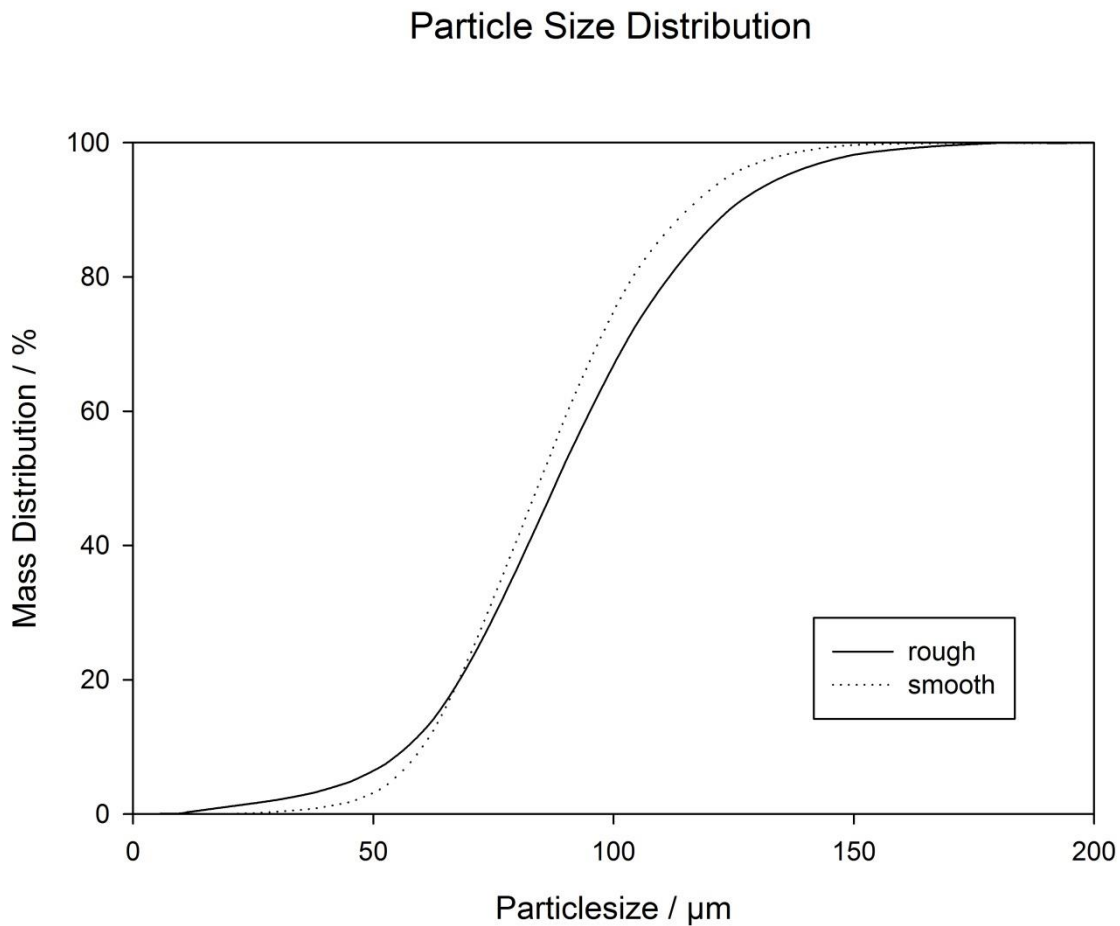


Figure 20: Particle size distribution of the rough and smooth powder determined by laser diffraction, n=3, MV

From these results the characteristic particle diameters of the samples were determined and are shown in Table 3.

Table 3: Parameters of the PSD, n=3, MV ± SD

	Smooth	Rough
X ₁₀ [μm]	59,5±0,156	56,32±0,243
X ₅₀ [μm]	84,85±0,155	88,39±0,325
X ₉₀ [μm]	117,27±0,550	124,34±0,454

Table 3 shows that the PSDs of both powders do not differ significantly. Moreover, the PSDs reveal that the particles exhibit a diameter ranging between 63 μm and 125 μm. Thus, the size fractions prepared by sieving are in the desired range.

3.1.3 Roughness

The powders were pictured using SEM (according to chapter 2.2.2.2) in order to assess surface roughness.

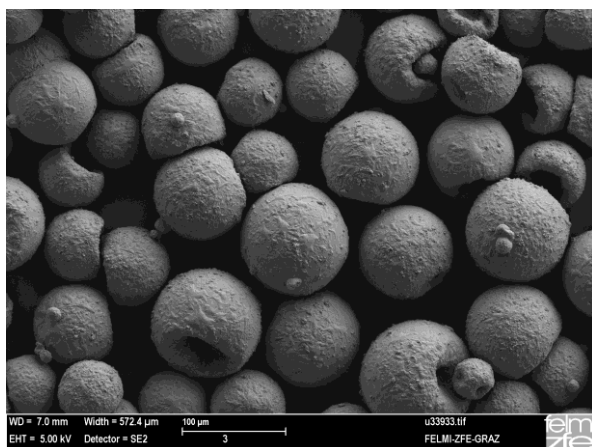


Figure 21: Scanning electron micrograph of the smooth powder

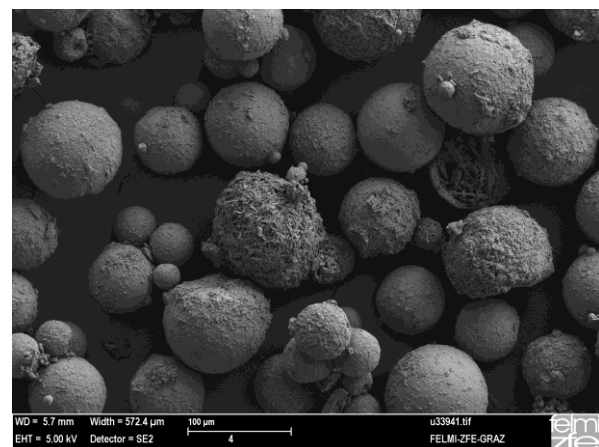


Figure 22: Scanning electron micrograph of the rough powder

The particles in Figure 21 are uniformly smooth, in contrast to that the particles in Figure 22 show qualitatively, partly higher roughness.

3.1.4 Specific Surface Area

The specific surface of the powders was evaluated (according to chapter 2.2.2.6), since the smooth and the rough powder were expected to exhibit different specific surface areas due to different surface roughnesses. The rough powder showed a higher specific surface area ($0.5930 \pm 0.007 \text{ m}^2/\text{g}$) in comparison to the smooth powder ($0.3868 \pm 0.0046 \text{ m}^2/\text{g}$), which –given the same particle size- has been expected. However according to findings by Littringer et al (2012), who provided the powders examined in the present study, the particles are porous and the crust of the particles might be gas permeable or partly gas permeable. Therefore, the BET measurements should be treated with caution and are not an exact indicator for surface roughness.

3.1.5 Bulk and tapped density

Since there is a different surface roughness probably causing differences in packing densities and flowability, the bulk and tapped densities were determined (according to chapter 2.2.2.5).

In Table 4 the values of the bulk and tapped densities are summarized

Table 4: Bulk and Tapped density, n=3, MV ± SD

	Bulk Density [g/ml]	Tapped Density [g/ml]
smooth	0.496 ± 0.006	0.588 ± 0.000
rough	0.403 ± 0.004	0.484 ± 0.000

It's likely that the differences of the bulk and tapped densities between the rough and the smooth powder are caused by different formations of the packing of the spheres. That means for a lower bulk and tapped density the spheres are packed more compact than for higher bulk and tapped densities, respectively. Since the calculation of the bulk and tapped density is the ratio between the weighed mass and the measured volume in the measuring cylinder, the higher volume leads to smaller bulk and tapped densities. Examination of the bulk and tapped densities revealed a higher bulk as well as tapped density of the smooth powder. This is not really unexpected since it is comprehensible that nicely smooth particles reach a closer packing of spheres. This is on the one hand caused by mechanical interlocking of the rough particles and on the other hand by the fact that every roughness generates more space for air within the powder bulk than a smooth surface. Another reason for differences in bulk and tapped densities might be differences in particle densities. Investigations on the particle density will be the subject of the following chapter.

Furthermore the Hausner ratio was determined according to Equation13.

$$\text{Hausner - ratio} = \frac{\text{tapped density}}{\text{bulk density}}$$

Equation13: Hausner Ratio

The Hausner ratio of the smooth powder is 1.186 ± 0.014 and of the rough powder 1.202 ± 0.011 .

3.1.6 Powder Density

Based on the findings of the investigations of the bulk and tapped densities the powders may differ with respect to particle density. Particle density was determined according to chapter 2.2.2.4.

For the smooth powder a density of $1.3386 \pm 0.0005 \text{ g/cm}^3$ and for rough powder a density of $1.4903 \pm 0.0018 \text{ g/cm}^3$ was determined. However according to Littringer et al. (2011) particles of both powders are hollow and their shell may be gas permeable making particle density determinations via gas pycnometry not very reliable.

3.1.7 Flowability

As another indicator of flowability the uniformity of the powder release from the dry powder inhaler was determined according to section 2.2.2.7. Figure 23 shows the mass of powder released per actuation for the smooth and for the rough powder, respectively.

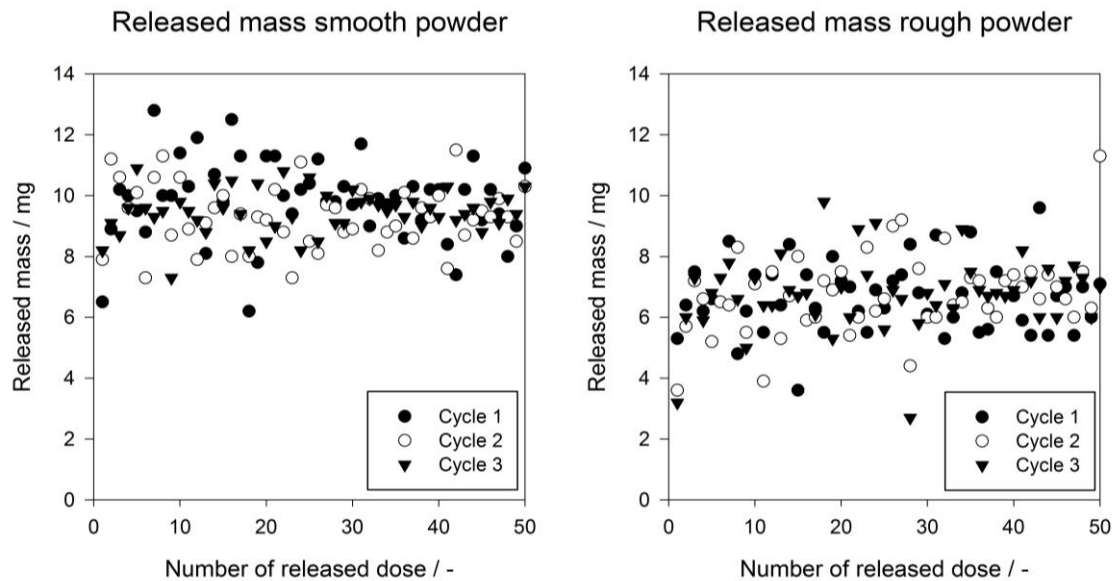


Figure 23: a) Released mass smooth powder; b) Released mass rough powder

The smooth powder shows a significantly higher released mass of 9.543 ± 1.031 mg compared to the rough powder (6.728 ± 1.231 mg) (see Table 5 and Table 6). Based on the findings of the bulk and tapped density (see chapter 2.2.2.5) the smooth powder has a higher bulk and tapped density, therefore, it can be concluded that a higher bulk and tapped density leads to a higher released mass.

A measure for the uniformly released mass is the deviation of the released mass. Therefore, the standard deviation of the released mass of each cycle and its mean were calculated.

In Table 5 and Table 6 the results of the smooth and rough powder are shown. The mean of the three standard deviations of the three cycles is lower for the smooth powder (i.e., 1.031 mg) than for the rough powder (i.e., 1.231 mg).

Table 5: Released mass smooth powder

	Cycle 1	Cycle 2	Cycle 3	Mean	SD
	[mg]	[mg]	[mg]	[mg]	[mg]
Mean	9,858	9,316	9,454	9,543	0,282
SD	1,350	1,025	0,718	1,031	0,316

Table 6: Released mass rough powder

	Cycle 1	Cycle 2	Cycle 3	Mean	SD
	[mg]	[mg]	[mg]	[mg]	[mg]
Mean	6,650	6,756	6,778	6,728	0,068
SD	1,146	1,314	1,234	1,231	0,084

3.2 Measurement of Electrostatic Charge of Mannitol without API in a stainless steel vessel

Measurements of charge uptake of the pure powders during the mixing process were carried out using stainless steel vessels according to chapter 2.2.3.1. The smooth powder has a specific charge of 0.05 ± 0.009 nC/g and the rough powder has a specific charge of 0.25 ± 0.0189 nC/g. For the statistical analysis a two tailed student-t test was performed. The two tailed student t- test showed a P value of < 0.001 . The mean value \pm the standard deviation of the charge magnitudes is plotted in Figure 24.

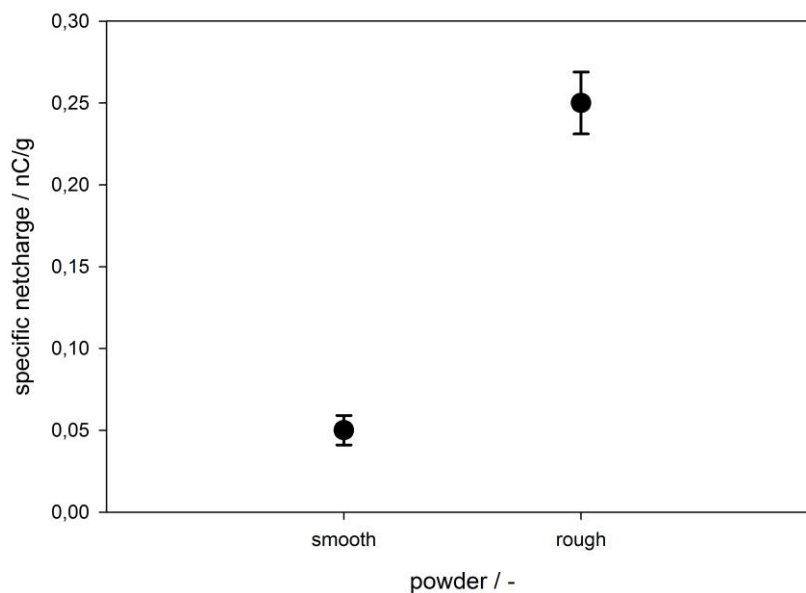


Figure 24: Electrostatic charge carried by mannitol in stainless steel vessel without API, n=3 (MV \pm SD)

The smooth mannitol powder showed a significantly lower charge than the rough powder in the stainless steel vessels. Although specific surface area measurements do not only evaluate the outer surface but also the inner one (see chapter 3.1.4), the

higher surface roughness of the rough powder (see chapter 3.1.3) is expected to yield in a higher surface area. That means that the rough powder has a higher specific surface area, that may take up more charges before charge saturation impedes further charge uptake.

3.3 Measurement of Electrostatic Charge with API in a stainless steel vessel

To complete the powder studies, Mannitol (i.e., carrier) and SS (i.e., model API) were mixed at a ratio of 1:40 according to chapter 2.2.4. The results of the charge experiments of these adhesive mixtures using rough mannitol powder and smooth mannitol powder as carriers did not show any significant differences. Both mixtures showed the same electrostatic charging behaviour and the charge ranged in the region of 0.2 nC/g (see Figure 25).

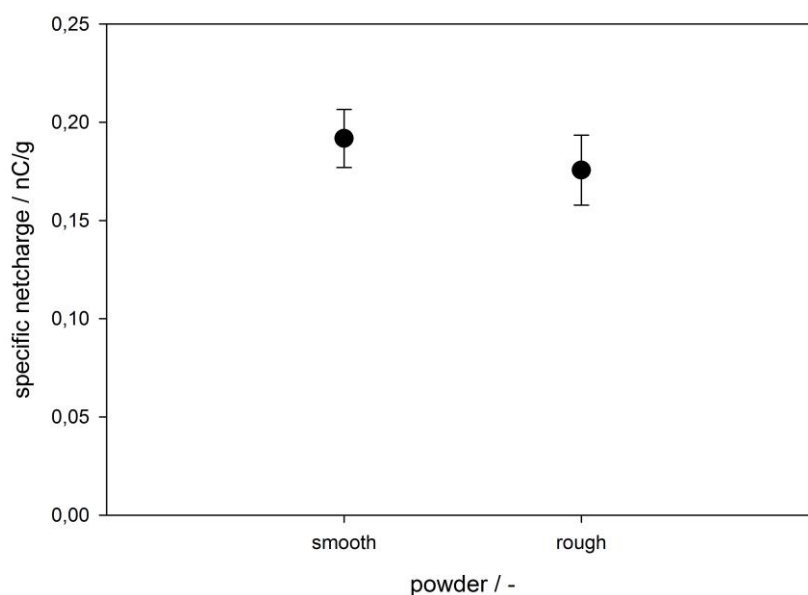


Figure 25: Electrostatic Charge carried by mannitol in Stainless steel vessel with API, n=3
(MV±SD)

According to the performed experiments without API, there should be a difference in charging of the powder mixtures due to the different charging characteristics of the smooth and rough mannitol. However, the SS particles may be located surrounding the mannitol particles. These fine API particles act like spacers between the mannitol particles and the vessel walls and may impede the direct contact between mannitol and vessel walls. Therefore contact to the vessel walls takes place only via the SS particles. As the SS particles cover the mannitol particles irrespective of the smooth or rough mannitol surface, charging behaviour does not longer depend on the characteristics of the mannitol particles.

3.4 Measurement of the Mixing Uniformity

To investigate the mixing uniformity, the experiments were performed according to chapter 2.2.5.

In Table 7 all statistical data of the mixing uniformity are summarized.

Table 7: API content of the samples taken from 3 independent adhesive mixtures (mean \pm SD of n=10)

	Mean [mg/g]		SD [mg/g]	
	smooth	rough	smooth	rough
Mixture 1	24.406	24.303	0.51	0.94
Mixture 2	24.603	24.279	0.47	0.38
Mixture 3	24.668	24.678	0.30	0.89
Mean	24.559	24.420	0.43	0.74
SD	0.14	0.22	0.11	0.31

The mixtures using the rough mannitol showed a mean standard deviation of 0.74 mg/g and using the smooth mannitol showed a mean standard deviation of 0.43 mg/g (see Figure 26).

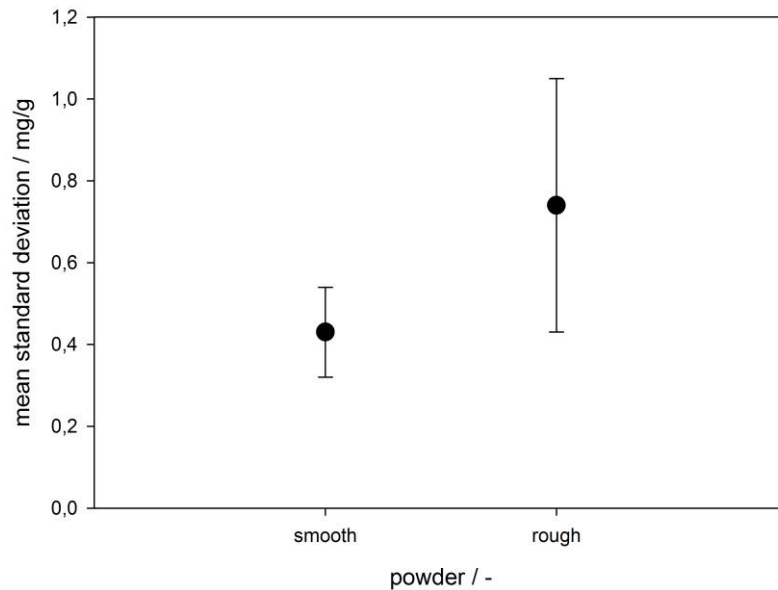


Figure 26: Mean standard deviation of the API content ($MV \pm SD$, $n=3$)

According to Adi et al. (2010) and Elajnaf et Al. (2006) it was shown that mannitol and SS charge negatively in stainless steel vessels. Based on these findings it can be expected that a higher charge magnitude on the mannitol powder and stainless steel can lead to repulsive forces between mannitol and SS.

At the beginning of the mixing process, the carrier and API were separated. Smooth mannitol powder generates less strong repulsive force than rough mannitol powder because of the different charging behaviour of the two carriers (see chapter 3.2). That means smooth mannitol powder with lower charging magnitude provides a better mixing homogeneity compared to rough mannitol powder due to lower repulsive forces at the beginning of the mixing process.

4 Summary

First, the smooth and the rough mannitol powders were determined with respect to their strength, roughness, specific surface area, particle size distribution, flowability, helium density, bulk and tapped density. Secondly their electrostatic charging behaviour and mixing uniformity with the drug salbutamol sulphate were investigated. The strength of the particle was sufficient enough to continue further measurements. First the roughness was evaluated by qualitative SEM measurements. After the SEM measurements the specific surface area was determined via nitrogen adsorption. It was shown that there is a difference between both, the smooth and the rough mannitol powders. As the powder was sieved before, the PSD was between 63 – 125 μm . The bulk and tapped density revealed that the smooth powder has a higher bulk and tapped density than the rough powder.

The electrostatic charging behaviour of the powders after mixing without API revealed that rough mannitol powder showed a higher charge magnitude in stainless steel vessels than smooth mannitol powder

The investigation of the adhesive powder showed a difference in their mixing uniformity but no difference on their charging magnitude. One possible reason for a similar charging magnitude could be that the small API particles covered the larger carrier particle, which leads to a similar surface area of both, the rough and the smooth powders. A reason for a different mixing homogeneity could be that mixing uniformity is influenced by the charging behaviour of the carrier at the beginning of the mixing process.

5 Conclusion and Outlook

Concluding from that, it has been shown that surface roughness influences the electrostatic charge uptake. Charge uptake is higher for the rough carrier powder than for the smooth one. However charge uptake of adhesive mixtures containing the carrier and the API was similar for both carrier types, the smooth one and the rough one. Nevertheless a difference in the mixing uniformity of the adhesive mixtures was observed. Adhesive mixtures containing the smooth powder showed a better mixing uniformity than the one containing the rough powder. A reason for a different mixing homogeneity could be that mixing uniformity is influenced by the charging behaviour of the carrier at the beginning of mixing.

Continuing on this topic further research has to be done. First of all, more different particle surface roughnesses should be investigated for better understanding the influence of surface roughness on electrostatic charge acquisition. Also inhaler and mixing studies with different APIs or a different ratio between carrier and API should be performed in order to get a more comprehensive understanding of the dependence of mixing homogeneity on electrostatic charging. Furthermore, there are many other important parameters in technology, that may be impacted by electrostatic charging like the interparticle interactions between the API and the carrier which is crucial for API detachment from the carrier surface upon inhalation, which in turn is key for the amount of API reaching the target site namely the tiny airways of the deep lung.

6 Bibliography

- Adi, H., Kwok, P., Crapper, J., Young, P., Traini, D., Chan, H., (2010) Does Electrostatic Charge Affect Powder Aerosolisation? *Journal of pharmaceutical sciences*, Vol.99, 2455- 2461
- Carter, P. A., Cassidy, O. E., Rowley, G., & Merrifield, D. R. (1998).
Triboelectrification of fractionated crystalline and spray-dried lactose. *Pharmacy and Pharmacology Communications*, 4, 111–115.
- Clark, J. (2004). Retrieved June 24, 2010, from chemguide:
<http://www.chemguide.co.uk/physical/phaseeqia/raoultnonvol.html>
- Eilbeck, J., Rowley, G., Carter, P. A., & Fletcher, E. J. (1999). The effect of materials of construction of pharmaceutical processing equipment and drugdelivery devices on the triboelectrification of size fractionated lactose. *Pharmacy and Pharmacology Communications*, 5, 429–433.
- Eilbeck, J., Rowley, G., Carter, P. A., & Fletcher, E. J. (2000). Effect of contamination of pharmaceutical equipment on powder triboelectrification. *International Journal of Pharmaceutics*, 195, 7–11.
- Elajnaf, A., Carter, P., & Rowley, G. (2006). Electrostatic characterisation of inhaled powders: effect of contact surface and relative humidity. *European Journal of Pharmaceutical Sciences*, 29, 375–384.
- Gonda, I. (1992). *Physico-chemical principles in aerosol delivery*. Stuttgart Germany: Medpharm GmbH Scientific Publisher pp. 95–115.

-
- Greenspan, L. (1976, October 22). Humidity Fixed Points of Binary Saturated Aqueous Solutions. *Journal of Research of the National Bureau of Standards* Vol. 81A No.1 , January - February 1977 .
- Karner S., N.A. Urbanetz (2012), Arising of electrostatic charge in the mixing process and its influencing factors, *Powder Technology*. 226, 261–268.
- Karner S., N. A. Urbanetz (2011), The impact of electrostatic charge in pharmaceutical powders with specific focus on inhalation-powders, *Journal of Aerosol Science*. 42, 428–445
- Labiris, N. R., & Dolovich, M. B. (2003). Pulmonary drug delivery. Part I: physiological factors affecting therapeutic effectiveness of aerosolized medications. *British Journal of Clinical Pharmacology*, 56, 588–599.
- Lide, D. R. (Edition 2006 - 2007). *CRC Handbook of Chemistry and Physics*. Boca Raton, London, New York: CRC Press Taylor & Francis
- Littringer E.M., A. Mescher, S.G. Maas, P. Walzel, N.A. Urbanetz (2011), Influence of droplet size on the crystallization behaviour of aqueous d-mannitol solutions during spray drying, in: *ILASS2011 Conference Proceedings*, pp. 1–8.
- Littringer E.M., A. Mescher, S. Eckhard, H. Schröttner, C. Langes, M. Fries, et al., (2012), Spray Drying of Mannitol as a Drug Carrier—The Impact of Process Parameters on Product Properties, *Drying Technology*. 30 ,114–124.
- Lüttgens,G. (Edition 2005) *Statische Elektrizität*, ISBN 3-8169-2506-5
- Murtomaa, M., & Laine, E. (2001). Effect of surface coverage of a glass pipe by small particles on the triboelectrification of glucose powder. *Journal of Electrostatics*, 54, 311–320.
- Murtomaa, M., Mellin, V., Harjunen, P., Lankinen, T., Laine, E., & Lehto, V. P.

-
- (2004). Effect of particle morphology on the triboelectrification in dry powder inhalers. *International Journal of Pharmaceutics*, 282, 107–114.
- OIML R121, I. O. (1996). *The scale of relative humidity of air*. Paris: Bureau International de Métrologie Légale.
- Rowley, G. (2001). Quantifying electrostatic interactions in pharmaceutical solid systems. *International Journal of Pharmaceutics*, 227, 47–55.
- Saint-Lorant, G., Leterme, P., Gayot, A., & Flament, M. P. (2007). Influence of carrier on the performance of dry powder inhalers. *International Journal of Pharmaceutics*, 334, 85–91.
- Steckel, H., & Bolzen, N. (2004). Alternative sugars as potential carriers for dry powder inhalations. *International Journal of Pharmaceutics*, 270, 297–306.
- Stieß, M. (Edition 2008). *Mechanische Verfahrenstechnik-Partikeltechnologie 1*, ISBN 978-3-540-32551-2
- Watanabe H., A. Samimi, Y.L. Ding, M. Ghadiri, T. Matsuyama, K.G. Pitt, Measurement of Charge Transfer due to Single Particle Impact, *Particle & Particle Systems Characterization*. 23 (2006) 133 – 137
- Watanabe H., M. Ghadiri, T. Matsuyama, Y.L. Ding, K.G. Pitt, H. Maruyama, et al., Triboelectrification of pharmaceutical powders by particle impact, *International Journal of Pharmaceutics*. 334 (2007) 149 – 155

7 Appendix

